Dilepton production by protons on nuclei and the partonic origin of depletion at small momentum fraction

K. E. Lassila
High Energy Physics Division, Argonne National Laboratory, Argonne, Illinois 60439
and Physics Department and Ames Laboratory, Iowa State University, Ames, Iowa 50011

U. P. Sukhatme
Physics Department, University of Illinois, Chicago, Illinois 60680

A. Harindranath
Department of Physics, Ohio State University, Columbus, Ohio 43210

J. P. Vary
Department of Physics, Iowa State University, Ames, Iowa 50011
(Received 13 September 1990)

We discuss and extend our previous predictions of dilepton depletion at small target parton momentum fraction in proton-nucleus collisons. These predictions were based on an analysis of the partonic origin of the European Muon Collaboration effect in deep-inelastic scattering (DIS) in a treatment of nuclei allowing multiquark clusters to be formed. With this input, we calculate the ratio of dimuons produced on nuclei to those produced on free nucleons. We obtain excellent agreement with data from a recent experiment, emphasizing that all input information came from our previous DIS analysis. Our calculations predict that beyond the range of presently measured data, there will be considerable dependence on the momentum carried by the annihilating parton in the incident proton.

I. INTRODUCTION

Experiments by the European Muon Collaboration (EMC) have shown that quarks in nuclei behave differently from those in free nucleons [1]; and, this effect has been corroborated by a number of experiments with both electron and muon beams [2]. A dominant feature of these data is a pronounced reduction in the value of $F_2^A(x)$, the deep-inelastic structure function per nucleon measured on a nucleus (A), at small momentum fraction $x<0.1$, relative to the corresponding quantity measured on deuterium (D), $F_2^{\rm D}(x)$. Except for $x>0.7$, which is beyond the range we discuss here, $F_2^{\rm D}(x)$ very nearly behaves like and is often assumed to be $2F_2(x)$ for two free nucleons. The ratio of these two quantities, $F_2^A(x)/F_2^{\rm D}(x)$, will be abbreviated $R_\gamma(A/{\rm D})$, with the subscript designating the virtual photon that couples to the charge of the quark (q). Data on different A targets show that $R_\gamma(A/{\rm D})<1$ for $x\lesssim 0.1$, reaches a maximum with $R_\gamma(A/{\rm D})\geq 1$ near $x=0.15$, attains another pronounced reduction below unity near $x=0.6$, and finally rises so that $R_\gamma \gg 1$ as $x\to 1$. It was shown [3] that parton effects resulting from clustering of nucleons to form color-singlet Nq structures ($N=6,9,\ldots$) gave contributions at all values of x very much like the observed deviations of $R_\gamma(A/{\rm D})$ from unity. This approach [3] continued from earlier works [4] but used data on $N=2$ and $N=3$ quark systems (mesons and nucleons) to deduce a plausible motivation for the properties of the $N=6$ system. This led to predictions for the value and slope of R_γ at $x=0$. In this paper we will further study the predictions that are implied by the phenomenological parton distributions of Ref. [3]; and, we argue that since the small-x behavior of R_γ is of partonic origin in this description our choice of parton distribution functions necessarily implies a small-x depletion of Drell-Yan pairs produced on nuclear targets.

It appears that many effects contribute to these differences between bound and free nucleons and it is important to understand them all because nuclear target data give us much of the input from which the nucleon structure functions are determined. Here, we study the contributions from multiquark [3] clusters to the differences between free and bound electrons, but first we discuss other contributions to develop a feeling for how they are related to one another. (i) Fermi motion is well studied but still raises questions. The Fourier transform of the wave function for a nucleon in the nucleus determines the momentum distribution of the nucleon in a bound state, in turn distorting the collision kinematics from that with the nucleon at rest [5]. This produces a rapid rise in the ratio $R_\gamma(A/{\rm D})$ at large x because the distributions in the denominator of this ratio become small compared to those in the numerator as $x\to 1$. (ii) Multiquark cluster probabilities can be calculated as the overlap of one nucleon with others [6], and the behavior of a particular quark or gluon in such an enlarged quark system (cluster) will necessarily be different than it is in a single nucleon. (iii) Since pions are exchanged between nucleons, the deep-inelastic process will occasionally

probe pions and consequently produce a distortion which must likewise be taken into account [7]. (iv) The bound-state character of the probed nucleon in the nucleus leads to a rescaling of the definition of the parton momentum fraction distribution. Numerous earlier studies of this specific contribution are discussed in Ref. [8] with the conclusion reached that "the nuclear binding and the nucleon Fermi motion in the convolution model of nucleons cannot explain the EMC effect." (v) Overlapping of the parton wave functions in *adjacent nucleons* can occur when the partons have very small-x values [9]. If we were to introduce an x dependence for cluster formation adjusted so the probability of forming a cluster decreases as a parton's momentum fraction becomes very large, the features of the small-x results of Ref. [9] could be accurately reproduced. (vi) Hypothetical Q^2 rescaling effects for a bound nucleon may also contribute in certain kinematic regions [10]. (vii) It has been argued that nucleon correlations contribute to the EMC effect [11]. We believe that there is overlap between cluster effects and correlations as both address phenomena at small baryonic separation distances. In fact, most of the above effects are not mutually exclusive, e.g., in an extended version of the quark-cluster model, an expansion of nuclear observables in terms of a complete set of three-quark ($3q$), ($6q$), ($9q$), ($12q$), etc., states may be able to account for all the data.

It would be surprising if any one of the above effects alone accounted for the structure of $R_\gamma(A/\mathrm{D})$ especially since some of them have a dominant contribution in a specific kinematic regime. It is consequently important to understand all these effects and to appreciate where the physics is overlapping. It is difficult to separate these different effects; but, because of our success in treating DIS at all x [3], we assume here they can be represented adequately within our choice of cluster parametrization. Therefore, we will emphasize multiquark clusters, since from the viewpoint of the (Nq)-state expansion many of the studied effects [5–11] will be included, at least partially. As further support, it has been shown that effects in backward production of protons and pions in neutrino reactions which had been attributed to nucleonic correlations can be understood logically as the by-products of multiquark fragmentation [12].

Our treatment of multiquark clusters will follow the approach in Ref. [3] where deviations of $R_\gamma(A/\mathrm{D})$ from unity were shown to result from differences in the regions of z in which valence $V(z)$ or ocean $O(z)$ quarks in N-quark clusters make their contributions. We denote by z the scaled momentum fraction, e.g., $z=x$ for the $3q$ nucleon and $z=x/2$ for a $6q$ two-nucleon color-singlet cluster since a given quark can have a maximum value $x=2$. For a generic N-quark cluster we write [3]

$$\begin{aligned} O_N(z)&=A_N(1-z)^{a_N}\ , \\ V_N(z)&=B_N\sqrt{z}\,(1-z)^{b_N}\ , \\ G_N(z)&=C_N(1-z)^{c_N}\ , \end{aligned} \tag{1}$$

for the ocean, valence, and gluon distributions, respectively. The six parameters in Eq. (1) were determined from normalization to N valence quarks, momentum conservation constraints, and by examining data for $N=2$ (pion) and $N=3$ (nucleon) clusters to suggest a plausible ratio for the momentum in the ocean to that in valence quarks, independent of N. With the physically reasonable requirement that $a_N>b_N$, it is logical to take a_6 to be approximately in the range 11–13. This led to a satisfactory representation of the data [1,2] for the ratio $R_\gamma(A/\mathrm{D})$, which were characterized by the three parameter sets

$$\begin{aligned} A&=A(3,9,9,11)\ , \\ B&=B(3,9,10,11)\ , \\ C&=C(3,9,10,13)\ , \end{aligned} \tag{2a}$$

where the quantities in parentheses signify b_3,a_3,b_6,a_6, respectively. In the calculations to be presented we shall generalize b_3, the generic exponent of $(1-z)$ for the nucleon valence quarks, to be $b_{3u}=3$ for the u quark and $b_{3d}=4$ for the d quark. This has no effect on the analysis in Ref. [3], and little effect on the present work. Thus, the content of Eq. (2a) is best rewritten

$$\begin{aligned} A&=A([3,4],9,9,11)\ , \\ B&=B([3,4],9,10,11)\ , \\ C&=C([3,4],9,10,13)\ , \end{aligned} \tag{2b}$$

where the numbers in parentheses signify $[b_{3u},b_{3d}],a_3,b_6,a_6$. The gluon functions will not be required in the present work. Each of these three sets of values (A,B,C) led to values or $R_\gamma(A/\mathrm{D})$ at $x\simeq 0$ which were less than unity. In numerical evaluations these three sets of parameters are specified as (A,B,C). Curves for case A will not be presented here because its predictions for the Drell-Yan (DY) ratios are very similar to those for case B.

II. THE DRELL-YAN EFFECT FOR PROTONS ON NUCLEI

It has been pointed out that the Drell-Yan process can be a good source of information on quark and antiquark structure functions in nuclei [13,14]. For our purposes, it is clear that if nucleons in nuclei form quark clusters, there should be evidence of them in $q\bar{q}$ annihilation to lepton pairs in hadron-nucleus collisions. The authors of Ref. [13] have already noted this, and their calculations used the parton distributions of Carlson and Havens [4] which resulted in considerable enhancement near $x=0$. We are, in this paper, effectively updating Ref. [13] with the more recent input provided by Ref. [3]. This input is such as to cause a depletion at low x in the EMC experiments. This depletion (sometimes referred to as "shadowing") results from the interplay between nucleon and cluster contributions in the nucleus.

The notation we use is standard [13], and we will give the translation to the notation introduced in the recent paper from the Fermilab experiment E772 [15]. We take x_1 (x_P in Ref. [15]) as the momentum fraction of the projectile (proton) that is carried by the annihilating quark

(antiquark) and x_2 (x_t in Ref. [15]) as the momentum fraction carried by the antiquark (quark) that was annihilated in the target. The annihilation produces a photon of four-momentum squared, Q^2, equal to the mass squared, M^2, of the lepton pair into which the photon decayed. We write the double-differential cross section in these variables as a sum over all quark flavors a in the projectile

$$\frac{d^2\sigma}{dx_1 dx_2} = \frac{4\pi\alpha^2}{9M^2} \sum_a e_a^2 F_a(x_1,x_2) , \tag{3}$$

where e_a is the charge in units of proton charge, α is the fine-structure constant

$$F_a(x_1,x_2) = q_a^P(x_1)\bar{q}_a^t(x_2) + \bar{q}_a^P(x_1) q_a^t(x_2) . \tag{4}$$

The quark [antiquark] distributions in the incident proton (P) or in the target (t) for parton a are $q_a^{P \text{ or } t}(x_{1 \text{ or } 2})$ [$\bar{q}_a^{P \text{ or } t}(x_{1 \text{ or } 2})$]. With the transverse momentum of the lepton pair also neglected [15] the product, $x_1 x_2 = M^2/s = \tau$, where s is the hadron-hadron center-of-momentum frame energy squared. We have $x_F = x_1 - x_2$ as the fraction of the maximum possible momentum for the dilepton pair. For fixed x_1, we form the ratio of the Drell-Yan cross section per nucleon for target A divided by the corresponding quantity on target D and plot this ratio, $R_{\rm DY}(A/\rm D)$ as a function of x_2 to compare with experiment. In this ratio the Q^2 dependence from QCD predominantly cancels. In the target (A or D), the annihilating parton can be in a nucleon or a larger quark cluster. This probability for finding the neutron and proton overlapping to form a $6q$ cluster in the deuteron will be taken as 4% [6]. We comment in the next section on the sensitivity to a $6q$ cluster in the deuteron.

III. LEPTON PAIRS FROM PROTONS ON NUCLEI IN E772

A. Curves for $R_{\rm DY}(A/\rm D)$

The calculations we shall present are relevant for the discussion of the results of Fermilab experiment E772 [15] which detected lepton pairs produced by proton beams incident on various nuclear targets: carbon, calcium, iron, and tungsten. The results have been presented as a ratio relative to the corresponding yield from deuterons. Some of our calculations showing a depletion in dilepton production at small x were presented previously and brief reports were published in various Conference Proceedings [16–18]. We have indicated that any parton structure function approach which gives small-x shadowing in deep-inelastic scattering (DIS) necessarily gives shadowing in the Drell-Yan process also. Our results appeared to be in conflict with preliminary results from E772 [19] but are in close agreement with the final experimental results as we show here. For the DY processes, at very large x_1 we find that the value of $R_{\rm DY}(A/\rm D; x_2=0) = R_\gamma(A/\rm D; x=0)$ for the cluster contribution only; the other effects mentioned in Sec. I (e.g., pions) will modify this somewhat. In our present calculations we do not assume x_1 is large but sum over all partons in the projectile that might contribute. Because this sum will not factor the same way in the numerator and denominator for DY, these two ratios will be approximately equal rather than exactly equal.

In Figs. 1–4, we show the Drell-Yan ratios for specific x_1 values calculated from Eqs. (1)–(4) and compared with the data [15] for A = C, Ca, Fe, and W, respectively. The dotted-dashed line on Fig. 3 was calculated and presented by the E772 experimenters as the prediction of the cluster model based on *their assumptions* for parton distributions within clusters.

B. Interpretation of curves for different x_1

The problem of interpretation of curves calculated for different x_1 values is the same for each target. We begin with $R_{\rm DY}(\rm C/D)$ vs x_2 curves in Fig. 1 and apply the same analyses of curves to the other targets. Carbon consists of 6 neutrons and 6 protons and we take the probability of cluster formation to be $f_{\rm C} \approx 0.1$ [6]. The behavior of $R_{\rm DY}(\rm C/D)$, like any of the $R_{\rm DY}(A/\rm D)$, is such that for $x_2 > 0.1$–0.2, the value of $R_{\rm DY}$ increases as x_1 increases. From the information available in Ref. [15], it appears certain that the value of $x_1 = 0.4$ is large compared to most of the E772 data. Therefore, a number of curves for

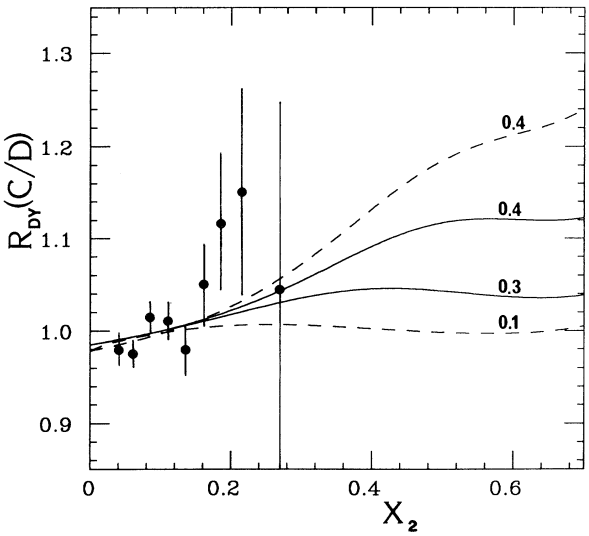

FIG. 1. Data [15] compared with theoretical curves for $R_{\rm DY}(\rm C/D)$ vs x_2 calculated for cases defined in Eqs. (1) and (2) with B given by the dashed lines and C given by the solid lines for the values of x_1 as given on the curves. Curves for case A are the same as those for B for values of $x_2 < 0.4$ and differ very little from B for larger x_2. In the text we refer to the dashed curves as $B(x_1=0.1)$ and $B(x_1=0.4)$, with the solid curves being $C(x_1=0.3)$ and $C(x_1=0.4)$. The curve labeled $x_1=0.3$ may be interpreted as a single representation of the theory for comparison with the data in this and subsequent plots for reasons discussed in the text.

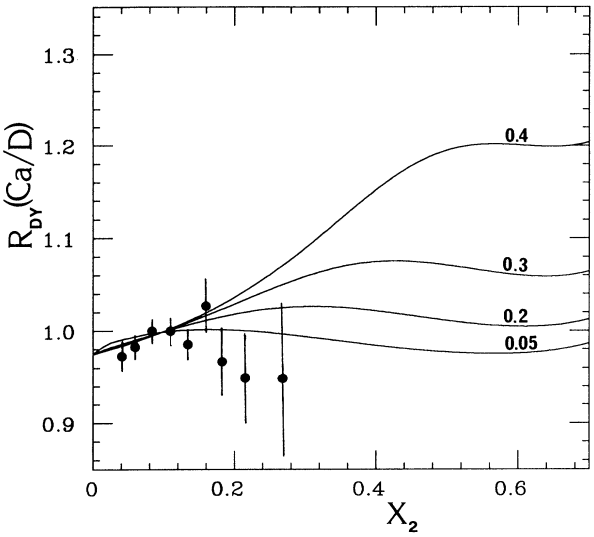

FIG. 2. Data [15] compared with cluster predictions of R_{DY}(Ca/D) vs x_2 for case C with $x_1=0.05, 0.2, 0.3, 0.4$. Curves for the other two cases in Eq. (2) will give an equally good description of this data.

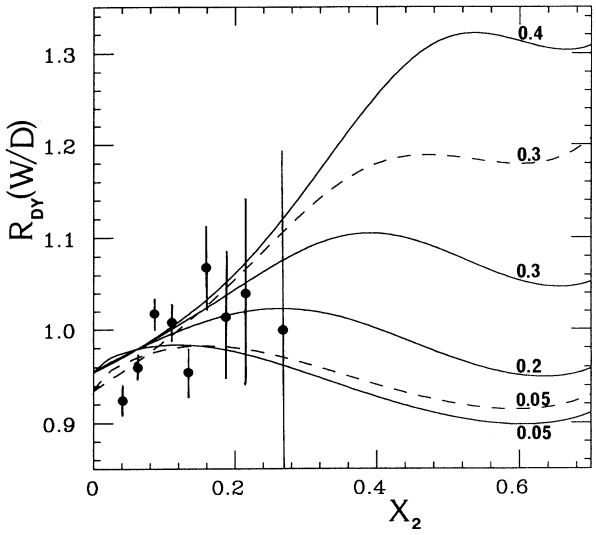

FIG. 4. Data [15] compared with cluster predictions of R_{DY}(W/D) vs x_2 for case C (solid lines) with $x_1=0.05, 0.2, 0.3, 0.4$ and for case B (dashed lines) with $x_1=0.05, 0.3$.

cases B and C for several different $x_1 \leq 0.4$ are shown compared with this data. Our presentation neglects the appropriate weighting of x_1 results for each x_2 bin because it is difficult to deduce the experimental weighting from Ref. [15]. Fortunately, the theory curves are very insensitive to the values for $x_1 \leq 0.4$ in the range where precision data exists. An excellent representation of the data will follow regardless of how the data are distributed in x_1. The curves clearly predict depletion of dilepton pairs at small x_2, an effect confirmed at roughly the $2\frac{1}{2}$-standard deviation level by the two smallest-x_2 data points in Fig. 1. We show one curve explicitly for $x_1=0.3$ because, as discussed below, this value can be interpreted as possibly being an effective average. This curve $C(x_1=0.3)$ is more than adequate to represent the data. However, we emphasize again that whatever the correct weighting factor for doing an integration on x_1 from 0.05 to 0.4 or larger, the data will be well described by quark clusters in the nucleus as illustrated in Fig. 1. We leave open the possibility that the additional effects discussed in Sec. I which might not overlap much with the cluster expansion can be included and yet have the same or better agreement with these data.

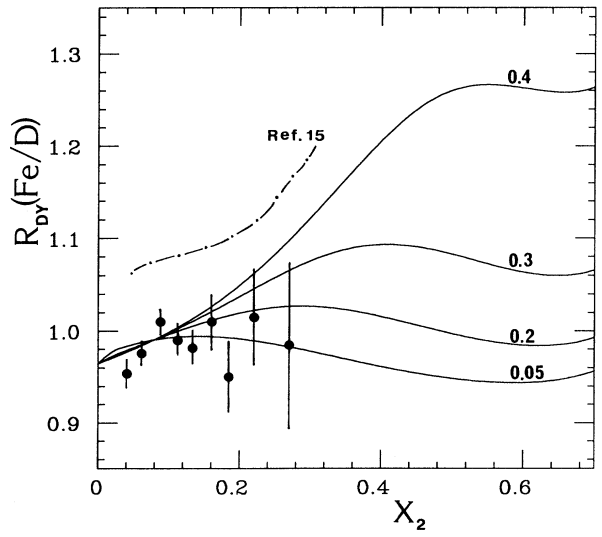

FIG. 3. Data [15] compared with cluster predictions of R_{DY}(Fe/D) vs x_2 for case C with $x_1=0.05, 0.2, 0.3, 0.4$ (solid lines). The high dotted-dashed curve represents our sketch of the "quark cluster" curve given in Ref. [15].

At this point, it is useful to comment on the experimental dilepton mass distribution. Reference [15] shows $d\sigma/dM$ falling by 2 orders of magnitude between $M=4$ and 9 GeV. If one normalizes to the cross section at any M value in this range, then the well-known $1/M^3$ scaling dependence multiplied by $\ln\ln(Q^2/Q_0^2)$ with $Q_0^2=4$ GeV^2 gives a good representation of this nonresonant region data. Therefore, any theoretical description of this Drell-Yan process which is calculated from a QCD-based interaction or parametrization of parton structure functions will be consistent with the $d\sigma/dM$ vs M dependence of the dilepton pairs. In particular, quarks and gluons in nucleons or $6q$ clusters in nuclei will likewise lead to this relative mass variation.

We have examined a number of different approaches to the x_1 distribution in the data which give results consistent with each other. First, using only Ref. [15], with $x_1=M^2/(x_2 s)$ and the experimental [15] range on x_2 ($0.04<x_2<0.27$, see Fig. 1) for a given M value we calculate the range of x_1 values, e.g., for $M=4$ GeV,

$0.04 \leq x_1 \leq 0.26$. Since the cross section is the largest at $M=4$, this range of x_1 receives the most weight in an averaging process based on $d\sigma/dM$; larger M will extend to larger x_1. With this interpretation, the curves for $x_1=0.3$ lie beyond the more important range of data and will be given in Figs. 1–4 to illustrate the upper end of the range of important variations. Another reason for emphasizing our calculations for $x_1=0.3$ is the fact that when we find the $d\sigma/dM$ weighted-mass average based on the cross-section curves in Ref. [15], this average mass corresponds to an average x_1 of $\langle x_1 \rangle = 0.3$.

According to Ref. [15], the x_F range of the data is $-0.03 < x_F < 0.6$, which should in principle, give some information relevant to $\langle x_1 \rangle$. If we interpret this as $x_F = x_1 - x_2$, then x_1 and x_2 will not vary symmetrically about $\sqrt{M^2/s}$ but will have $x_1 > \sqrt{M^2/s} > x_2$, except in the small experimental data range $-0.03 < x_F < 0$. The most precise data at small x_2 therefore can be seen to correspond to relatively small x_1 and we reach more or less the same conclusion as above.

Additional information on the variables appropriate to the data is available [19]. In the presentation of Ref. [19], a scatterplot of events from E772 showing x_2 versus x_1 for the high-mass setting and for the low-mass setting of the apparatus was presented. For the former setting, $\langle x_1 \rangle$ is close to 0.3, or conservatively between 0.3 and 0.35, while for the low-mass setting $\langle x_1 \rangle \sim 0.25$. Unfortunately, the data for the high-mass setting comprise *only* 6% of the total data sample. The conclusion again is that the analysis we present will give an unbiased comparison with the data. For each of Figs. 1–4, the proper theoretical curve to compare with each data set is a weighted average of contributions from x_1 bin values between ~ 0.04 and 0.5. Given the limited variation of these curves in the x_2 range of the data one can see that a completely adequate representation of the data will follow for any case in Eq. (2). In the comparison of case B with the carbon target data in Fig. 1, we should average over a set of dashed curves between the lower [$B(x_1=0.04)$ is very close to the plotted $B(x_1=0.1)$ curve] and upper dashed curves. The same conclusion is reached for case C for which only curves $C(x_1=0.3,0.4)$ are shown, with the appropriate lowest solid curve being close to the lower dashed curve. In view of this discussion, it is seen that a curve with $x_1=0.3$ serves as a reasonable curve on which to base comparisons between our model and the E772 data.

Yet another evaluation of what should be the correct weighting is obtained from the average masses given in Ref. [19] for each of the three ranges of E772 data. We conclude from some estimates we have made that nothing new can be added to the above analysis.

C. Comparison with data for heavier mass targets

Figures 2–4 show our theoretical curves for $R_{\rm DY}(A/{\rm D})$ versus x_2 for $A={\rm Ca}$, Fe, W for several x_1 values compared with data. As A increases, f_A increases and the depletion of events relative to D becomes more marked. The precise values for f_A cannot be predicted well; the values we used [6,13] are $f_{\rm Ca}=0.14$, $f_{\rm Fe}=0.18$, $f_{\rm W}=0.22$. There are strong indications that these probabilities should be larger for heavier nuclei as the calculations of Ref. [6] show that probabilities for the existence of $9q$, $12q$, etc., clusters grow with A. We are including the effects of these larger clusters in some approximate way. The dilepton pair ratio for the calcium target data is shown in Fig. 2, for $x_1=0.05$, 0.2, 0.3, 0.4 for case C [the other two cases in Eq. (2) give similar results]. From the previous subsection we note that the curve labeled as $x_1=0.3$ can be interpreted as the theory representation to be compared with the data. However, if we are to average these curves together with a weight function that falls rapidly to zero as x_1 increases beyond 0.3, an equally acceptable description of the data results. The effect of the $f_{\rm D}=0.04$ cluster fraction in the deuteron can be noted on $R_{\rm DY}({\rm Ca/D})$ for $(x_1=0.3, x_2=0)$: The plotted value of 0.975 decreases to 0.965 when $f_{\rm D}\to 0$. Thus, our consistent treatment of the deuteron with a $6q$ cluster included is not a major effect in our data analysis.

The comparison of the solid theory curves in Fig. 3 with data for $R_{\rm DY}({\rm Fe/D})$ versus x_2 proceeds exactly as the discussion for Fig. 2. An additional dotted-dashed curve is presented from Ref. [15] where the authors represent this curve as the prediction of the quark-cluster model [4] based without specifying how x_1 is treated. The parton distributions of Ref. [4] were based on crude assumptions and those early applications did not provide a strong test of the ocean and gluon distributions. Clearly, our curves which are based on a quark-cluster model, but with parton distributions determined by a more systematic approach to the hadron target data, disagree markedly with the dotted-dashed curve.

We note a very slow trend for the theory curves to show greater depletion or shadowing as x_1 increases. Conversely, for $x_2 > 0.1$, there is a slow increase of $R_{\rm DY}({\rm Fe/D})$ in the range of data as x_1 increases and this increase becomes dramatic beyond the range of data, a prediction of the cluster model.

The final data comparison, for tungsten $R_{\rm DY}({\rm W/D})$ versus x_2, is shown in Fig. 4. The curves for case C, $C(x_1=0.05)$, $C(x_1=0.2)$, $C(x_1=0.3)$, and $C(x_1=0.4)$, are shown as the solid lines. Two dashed curves for case B are also shown to illustrate the approximate spread of the theoretical error bands following from the small changes in the $6q$ cluster structure functions implied by the differences in the three cases given in Eq. (2). It is clear that a fairly good representation of the data results. We further note that if the probability of 6q clusters in tungsten is increased from $f_{\rm W}=0.22$ to $f_{\rm W}=0.3$, as could be appropriate for a heavy nucleus [4], the value of $R_{\rm DY}$ at $x_2=0$ decreases from 0.935 to 0.905 for case B, the dashed lines. Thus, the lowest x_2 point on Fig. 4 would be very well described without changing the comparison with the other data. In the framework of the cluster expansion this could amount to allowing enhanced shadowing of the type discussed by Qiu [9] to exist between soft partons in a cluster and partons in adjacent nucleons or clusters.

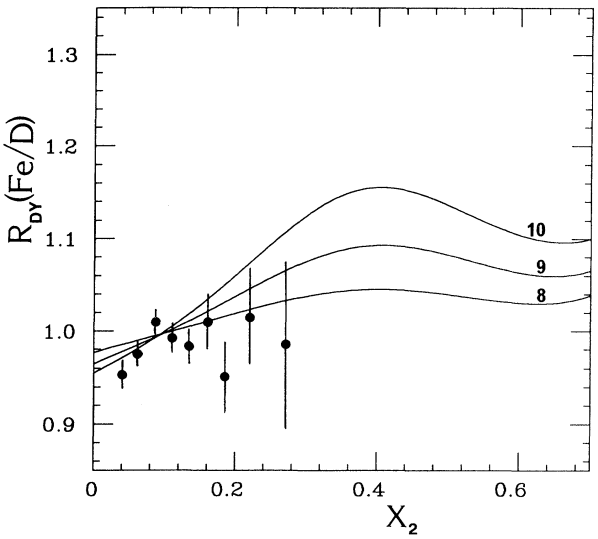

FIG. 5. Data [15] for R_{DY}(Fe/D) vs x_2 compared with curves for case $C([3,4],a_3,10,13)$ for $x_1=0.3$ to illustrate the effect of changing the power a_3 of the nucleon ocean distribution, $a_3=8,9,10$ as indicated on the appropriate curve.

D. Varying the nucleon sea

We have pointed out that one can naively use the ratio $R_{DY}/(A/D)$ versus x_2 for $x_1=0.3$ to compare directly with the data. Figure 5 illustrates the sensitivity of R_{DY}(Fe/D) at $x_1=0.3$ to changes in the power a_3 in $(1-z)^{a_3}$ of the ocean quarks in the nucleon as defined in Eq. (1). The three curves, labeled by the value of $a_3=8$, 9, 10 in Fig. 5, are different only because a_3 changes, being calculated for case $C([3,4],a_3,10,13)$, with the fraction of clusters for iron, $f_{Fe}=0.18$. For the curves in Fig. 5, the normalization of each ocean distribution is appropriately taken into account [3].

The comparison shown in Fig. 5 illustrates the interplay between nucleon sea and cluster contributions, as without clusters all curves would be flat (1.0). Consequently, the differences between them, especially at small x_2, argue for the need to determine the ocean distributions from data with isolated nucleon targets. To try to deduce the nucleon sea or ocean behavior at small momentum fraction from data while neglecting this interplay of cluster and nucleon contributions will likely lead to incorrect results. To elaborate, a typical sophisticated nucleon structure function parametrization has smaller and larger powers of x for the nucleon sea, perhaps $(1-z)^{7 \text{ or } 8}$ plus a term with $(1-z)^{10 \text{ or } 11}$. The fitting of data such as that shown in Fig. 5 to get at the nucleon sea necessarily requires removal of the quark-cluster effects before any reliable parametrization will be possible.

IV. CONCLUSION AND DISCUSSION

The curves in Figs. 1–4 all illustrate consequences of the existence of quark clusters in nuclei. As x_1 increases, the value of the ratio $R_{DY}(A/D)$ decreases slightly at $x_2=0$ and increases considerably at larger $x_2>0.2$. This strong x_1 dependence seems to be an untested prediction of the quark-cluster model. The data [15] are not sufficiently precise to study such an effect in any detail. Performing an experiment with enough statistics to allow bins in x_1 to be plotted would *increase* our knowledge about the behavior of quarks in nuclei. With quark clusters forming in nuclei, it is clear that the major part of the increase in shadowing near $x=0$ is explained by the increase in the number of possible quark clusters as the nucleon number increases. The values used, [6,13] $f_C=0.1$, $f_{Ca}=0.14$, $f_{Fe}=0.18$, $f_W=0.22$, were based on estimates of the overlap between nucleons from extrapolations in A, and have perhaps a 25% error in them. This produces a 0.03 change in the value of R_{DY} at $x_2=0$ for the heavy nuclei. This uncertainty in f_A might be large enough that for a heavy nucleus like W, $f_W=0.3$ is possible (Sec. III). This uncertainty reflects our approximate treatment of clusters of 9, 12, etc., quarks in such a nucleus. Another source of deviation in the theory value comes from the intrinsic uncertainties in deducing the structure functions and the resulting feedback in getting the cluster distributions accurately. From Fig 5 we would expect this to have a smaller effect than the 0.03 change following from the uncertainty in f, so perhaps the total theory error band on our R_{DY} curves might be such as to be 0.04–0.05 wide throughout most of the x_2 range of the data on the figures. We note that this 0.04 uncertainty in R_{DY} is small compared with the differences between our theory curves and the dotted-dashed curve in Fig. 3. We believe our curves are much more representative of the quark-cluster model predictions.

In conclusion, the comparison with Drell-Yan data and the earlier comparison with DIS data supports the use of the cluster model as a plausible phenomenological description of the behavior of quarks in nuclei. In the past, experimenters have usually treated the nucleus as a collection of free nucleons when extracting structure functions from nuclear target data. The cluster-model approach provides a tool with which to remove nuclear effects and get more reliable parton distributions. A prediction of the model can be seen in the data comparisons, there is considerable dependence on the momentum carried by the annihilating parton in the projectile proton beyond the range of existing E772 data.

ACKNOWLEDGMENTS

The first two authors are grateful for hospitality of and discussion with many colleagues at the HEP Division of Argonne National Laboratory where the majority of this work was done. We would like to acknowledge the support of the U.S. Department of Energy, Division of High Energy Physics, Contract No. W-31-109-ENG-38 and Grants Nos. DE-FG02-84ER40173, DE-FG02-87ER40371, and Contract No. W-7405-ENG-82 Office of Energy Research (KA-01-01) and the support of the National Science Foundation under Grant No. PHY-8719526.

[1] See, e.g., EMC Collaboration, J. Ashman *et al.,* Phys. Lett. B **202**, 603 (1988); J. J. Aubert *et al., ibid.* **123**, 275 (1983).
[2] R. G. Arnold *et al.,* Phys. Rev. Lett. **52**, 727 (1984); A. Bodek *et al., ibid.* **50**, 1431 (1983); **51**, 534 (1983); G. Bari *et al.,* Phys. Lett. **163B**, 282 (1985); A. C. Benvenuti *et al.,* Phys. Lett. B **189**, 483 (1987); J. J. Aubert *et al., ibid.* **259**, 189 (1985); **272**, 158 (1984).
[3] K. E. Lassila and U. P. Sukhatme, Phys. Lett. B **209**, 343 (1988).
[4] H. Pirner and J. P. Vary, Phys. Rev. Lett. **46**, 1376 (1981); C. E. Carlson and T. J. Havens, *ibid.* **51**, 261 (1983).
[5] A. Bodek and J. L. Ritchie, Phys. Rev. D **23**, 1070 (1981); **24**, 1400 (1981); see also D. Kusno and M. J. Moravcsik, *ibid.* **20**, 2734 (1978); G. Yen, J. P. Vary, A. Harindranath, and H. J. Pirner, Phys. Rev. C **42**, 1665 (1990) for earlier work and references.
[6] M. Sato, S. A. Coon, H. J. Pirner, and J. P. Vary, Phys. Rev. C **33**, 1062 (1986).
[7] E. L. Berger and F. Coester, Annu. Rev. Nucl. Part. Sci. **37**, 463 (1987); E. L. Berger, F. Coester, and R. B. Wiringa, Phys. Rev. D **29**, 398 (1984).
[8] G. L. Li, K. F. Liu, and G. E. Brown, Phys. Lett. B **213**, 531 (1988).
[9] A. H. Mueller and J. Qiu, Nucl. Phys. **B268**, 427 (1986); J. Qiu, *ibid.* **B291**, 746 (1987); E. L. Berger and J. Qiu, in *Topical Conference on Nuclear Chromodynamics,* edited by J. Qiu and D. Sivers (World Scientific, Teaneck, New Jersey 1988), p. 119; L. L. Frankfurt and M. I. Strikman, Phys. Rep. **160**, 235 (1988); N. N. Nicolaev and V. I. Zakharov, Phys. Lett. **55B**, 397 (1975).
[10] F. Close *et al.,* Phys. Rev. D **31**, 1004 (1985); F. E. Close, Nucl. Phys. **A478**, 407c (1988).
[11] C. Ciofi degli Atti and S. Liuti, Phys. Lett. B **225**, 215 (1989).
[12] C. E. Carlson, K. E. Lassila, and U. P. Sukhatme, Phys. Lett. (to be published).
[13] A. Harindranath and J. P. Vary, Phys. Rev. D **34**, 3378 (1986).
[14] E. L. Berger, Nucl. Phys. **B267**, 231 (1986); R. P. Bickerstaff, M. C. Birse, and G. A. Miller, Phys. Rev. Lett. **53**, 2532 (1984); Phys. Rev. D **33**, 3228 (1986); W.-Y. P. Hwang and L. S. Kisslinger, Phys. Rev. D **38**, 788 (1988).
[15] D. M. Alde *et al.,* Phys. Rev. Lett. **64**, 2479 (1990).
[16] K. E. Lassila and U. P. Sukhatme, in *Nuclear and Particle Physics on the Light Cone,* edited by M. Johnson and L. Kisslinger (World Scientific, New Jersey, 1989) p. 115.
[17] K. E. Lassila, A. N. Petridis, C. E. Carlson, and U. P. Sukhatme, in *Proceedings of the American Physical Society Division of Particles and Fields Meeting at Rice University,* edited by W. Bonner and H. E. Miettinen (World Scientific, New Jersey, 1990), p. 593.
[18] K. E. Lassila and U. P. Sukhatme (unpublished).
[19] J. C. Peng, *Nuclear and Particle Physics on the Light Cone,* in talk presented at the LAMPF Workshop, edited by M. Johnson and L. Kisslinger (World Scientific, New Jersey, 1989), p. 65.